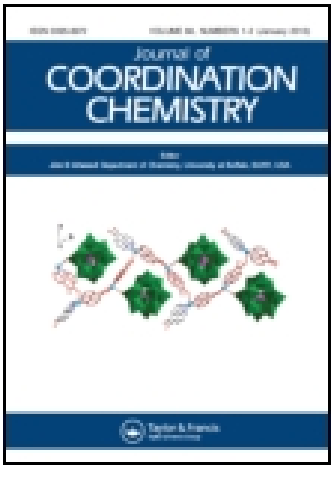

Journal of Coordination Chemistry
Publication details, including instructions for authors and subscription information:
http://www.tandfonline.com/loi/gcoo20

On construction of lead coordination polymers derived from N′-(2-hydroxybenzylidene)nicotinohydrazide via covalent and non-covalent interactions

Agata Trzesowska-Kruszynska[a]
[a] Department of X-ray Crystallography and Crystal Chemistry, Institute of General and Ecological Chemistry, Lodz University of Technology, Lodz, Poland

Accepted author version posted online: 09 Jan 2014.Published online: 27 Jan 2014.

To cite this article: Agata Trzesowska-Kruszynska (2014) On construction of lead coordination polymers derived from N′-(2-hydroxybenzylidene)nicotinohydrazide via covalent and non-covalent interactions, Journal of Coordination Chemistry, 67:1, 120-135, DOI: 10.1080/00958972.2013.876494

To link to this article: http://dx.doi.org/10.1080/00958972.2013.876494

Journal of Coordination Chemistry, 2014
Vol. 67, No. 1, 120–135, http://dx.doi.org/10.1080/00958972.2013.876494

On construction of lead coordination polymers derived from *N′*-(2-hydroxybenzylidene)nicotinohydrazide via covalent and non-covalent interactions

AGATA TRZESOWSKA-KRUSZYNSKA*

Department of X-ray Crystallography and Crystal Chemistry, Institute of General and Ecological Chemistry, Lodz University of Technology, Lodz, Poland

(*Received 31 July 2013; accepted 5 November 2013*)

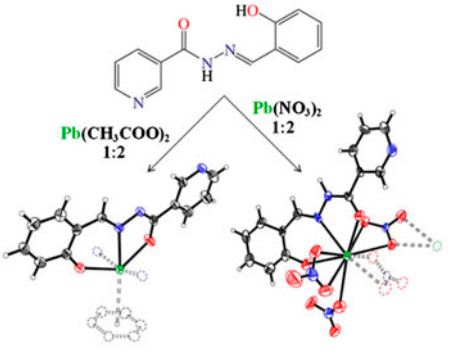

Lead(II) and lead(IV) coordination polymers with *N′*-(2-hydroxybenzylidene)nicotinohydrazide have been synthesized from lead(II) salts, and subsequently characterized by solid-state UV–Vis–IR spectroscopy, thermal analysis, and powder and single-crystal X-ray diffraction techniques. The compounds crystallize in the same space group but differ in the oxidation state of lead, composition, conformation of the organic ligand, its charge, and tautomeric form. The coordination network is propagated by the hydrazone anion in the lead(II) metal-organic framework *catena*-[(μ_2-*N*-((2-oxidophenyl)methylidene)pyridine-3-carbohydrazonoato-*N*:*N′*,*O*,*O′*)-lead(II) (**1**) and by nitrate in a one-dimensional lead(IV) coordination polymer *catena*-(μ_2-nitrato-O,O)-(nitrato-O,O′)-(salicylaldehydeisonicotinoylhydrazonato-N,N′,O)-lead(IV) nitrate (**2**). The formation of metal-organic framework of **1** is affected by Pb$\cdots\pi$ interactions.

Keywords: Lead(II), Lead(IV) coordination polymer; Holodirected and homodirected; Non-covalent interactions; Pb$\cdots\pi$ interactions; Metal-organic framework

*Email: agata.trzesowska@p.lodz.pl

1. Introduction

The coordination chemistry of nicotinoylhydrazones is diverse [1]. These compounds usually form coordination compounds by three aliphatic donors (i.e. N,O,O) with d- and f-block elements. There are also structurally characterized complexes of tetradentate nicotinoylhydrazones, in which the *N*-heterocyclic atoms are involved in coordination polymer formation, and pentadentate 2-pyridinecarboxylhydrazone possessing a metal coordinated to the N_2 bidentate donors of the ligand. The coordination chemistry of p-block element compounds with nicotinoylhydrazones is limited to tin coordination compounds.

In general, lead(II) coordination compounds have been studied due to the toxicity of this metal and the influence of the stereochemically active lone electron pair on the properties and stereochemistry of solid-state materials based on lead ions [2–10]. The molecular mechanism of toxic actions of lead is poorly known. Model ligands possessing S donors are used for the preparation of lead(II) complexes (mimicking the thiolate rich enzymes) to understand the lead-binding modes, crucial for designing selective chelating agents [11, 12]. Lead could interact with other target proteins, and thus multiple mechanisms of lead toxicity may exist. Thus, studies of bonding properties of lead and analysis of secondary interactions in lead compounds are necessary and interesting. Hence, the solid-state characterizations of two lead coordination compounds with nicotinoylhydrazone, as well as the results of quantum mechanical calculations explaining bonding properties of lead, are reported here.

2. Experimental

2.1. *Synthesis*

Equimolar quantities (10 mM) of nicotinic hydrazide and 2-hydroxybenzaldehyde were mixed. The mixture was stirred and heated on an electric hotplate in the absence of solvent and catalyst until the initially watery mixtures (from water evolving during reaction) solidified to products. The obtained *N*′-salicylidene-3-pyridinecarbohydrazide monohydrate was cooled and used without further purification.

A methanolic solution (50 cm^3) of *N*′-salicylidene-3-pyridinecarbohydrazide monohydrate (4 mM, 0.968 g) was added to an aqueous solution (10 cm^3) of lead(II) acetate trihydrate (2 mM, 0.755 g). The mixture was stirred for 30 min. The resulting yellow solution was left to stand at room temperature. After one week, an orange crystalline product, *catena*-[(μ_2-*N*-((2-oxidophenyl)methylidene)pyridine-3-carbohydrazonoato-*N*:*N*′,*O*,*O*′)-lead(II) (**1**), was filtered and dried in air. The compound is stable in air. An attempt to obtain the coordination polymer of lead(II) by solventless method was unsuccessful (on the basis of XRPD results). (**1**): m.p. 370 °C (decomposition starts after melting at 385 °C, figure S1 (see online supplemental material at http://dx.doi.org/10.1080/00958972.2013.876494)). Yield: 61% (based on Pb). Anal. Calcd for $C_{13}H_9N_3O_2Pb$ (%): C, 34.94; Pb, 46.41. Found (%): C, 34.36; Pb, 45.81.

Catena-(μ_2-nitrato-O,O)-(nitrato-O,O′)-(salicylaldehydeisonicotinoylhydrazonato-*N*,*N*′,O)-lead(IV) nitrate (**2**) was synthesized by the same procedure as **1**, only an aqueous solution (10 cm^3) of lead(II) nitrate(V) (2 mM, 0.661 g) was used instead of lead(II) acetate. After four days, bright yellow crystals of **2** were formed. (**2**): m.p. 217 °C (vigorous decomposition starts after melting at 240 °C, figure S1). Yield: 48% (based on Pb). Anal. Calcd for $C_{13}H_{10}N_6O_{11}Pb$ (%): C, 24.63; Pb, 32.71. Found (%): C, 24.21; Pb, 32.13.

2.2. *X-ray crystallography*

The crystals were mounted on a KM-4-CCD automatic diffractometer equipped with a CCD detector for data collection. X-ray intensity data were collected with graphite-monochromated Mo$K\alpha$ radiation with ω scan mode. The structures were solved by direct methods and subsequently completed by difference Fourier recycling. All non-hydrogen atoms were refined anisotropically using full-matrix least squares on F^2. The geometry of hydrogens bonded to carbon was idealized after each cycle of least-squares refinement. SHELXS97, SHELXL97, and SHELXTL [13] were used for all the calculations.

The X-ray powder diffraction patterns were measured in reflection mode on an XPert PRO X-ray powder diffraction system equipped with a Bragg–Brentano PW 3050/65 high-resolution goniometer and PW 3011/20 proportional point detector. The Cu$K\alpha_1$ radiation was used. The patterns were measured at 298.0 K in the 2θ range 5–90° (figure S2).

2.3. *Measurements*

IR spectra (400–4000 cm^{-1}) were recorded for samples prepared as KBr disks with a Jasco FT/IR-6200 spectrophotometer (figures S3 and S4). UV–Vis spectra were recorded with a Jasco V-660 spectrophotometer, in transmission mode, for solid-state samples pressed between two quartz plates. The positions of maxima were determined on the basis of 1st derivative of deconvoluted curves by Wiener algorithm (FWHM = 51). A differential scanning calorimeter (DSC 200 F3 *Maia*, Netzsch) was used to measure the m.p. of **1** and **2** under N_2.

Thermal analysis was carried out in a TG/DTA-SETSYS-16/18 thermoanalyser coupled with a ThermoStar (Balzers) mass spectrometer. The samples were heated in corundum crucibles up to 1000 °C at a heating rate of 5 °C min^{-1} in air. The final product of decomposition was calculated from TG curves (figures S5 and S6). The temperature range was determined by the thermoanalyser Data Processing Module [14].

2.4. *Theoretical calculations*

Calculations of Pb$\cdots\pi$ interaction energy were performed at the M06 [15] and at the second-order Møller–Plesset (MP2) [16] level of theory using the 6-31++G(d,p), aug-cc-pVQZ, and LANL2DZ ECP (for Pb) basis sets and GAUSSIAN03 [17] software. The geometrical parameters of Pb$\cdots$benzene moiety were employed from the crystal structure data. Basis set superposition error corrections were carried out using the counterpoise (CP) method of Boys and Bernardi [18]. For comparison, the geometry of Pb$\cdots$benzene was optimized at the M06 [15] level of theory using the 6-31++G(d,p) and LANL2DZ ECP (for Pb) basis sets. The molecular wave functions for the topological analysis of the electron density distribution [19] were calculated with the M06 density functional using the 6-31++G(d,p) and WTBS [20, 21] (for Pb, taken from EMSL Basis Set Exchange Library [22, 23]) basis sets.

3. Results and discussion

3.1. *The description of the structure*

The lead compounds were prepared by reaction of known *N*′-salicylidene-3-pyridinecarbohydrazide monohydrate [24] with lead(II) acetate and lead(II) nitrate, respectively.

The crystal structures were determined by single-crystal X-ray diffraction (table 1). The phase homogeneity of the obtained products was confirmed by powder X-ray diffraction by comparison of obtained reflection positions with the reference X-ray powder diffraction pattern calculated on the basis of the single-crystal structure (figure S2). Spectral and thermal analyses were performed for ligand and both coordination compounds in the same experimental conditions to allow comparisons.

Both compounds crystallize in the same space group and possess polymeric structures. The lead coordination sphere is completed by weak secondary interactions and can be classified as holodirected for **1** and **2**. The most important differences between compounds concern the oxidation state of lead, conformation of organic ligand, its charge, and tautomeric form. The coordination network is propagated by the hydrazone anion in **1** and by nitrate ions in **2**.

In the crystal structure of the homoleptic coordination polymer, $[Pb(C_{13}H_9N_3O_2)]_n$, (**1**) (figure 1), lead(II) cation is coordinated by one doubly deprotonated ligand through one phenolate oxygen atom, one imine nitrogen atom, one enolate oxygen atom, and by a second ligand through pyridine nitrogen atom, forming a 1-D zigzag chain along the crystallographic [0 0 1] axis. During complexation, the ligand changes its conformation by rotation around the C22–C6 bond; thereby the pyridine nitrogen is located on the opposite sides of the C6–O1 carbonyl bond, which is in contrast to the crystal structure of the pure ligand, *N*′-salicylidene-3-pyridinecarbohydrazide [24]. The ligand bond lengths in the complex are consistent with those in the uncoordinated hydrazone molecule [24] except for the C(O)N moiety (table 2). The C–N bond is shortened and the C–O bond is elongated in **1**, in comparison to free hydrazone. Such redistribution of π-electron density over the amide group is common [25–27]. The hydrazone anion is close to planar, with maximum deviation from the weighted least-squares plane calculated for all non-H atoms of 0.224(8) Å for C4. There is no classic hydrogen bond in the structure, since in the structure only C–H donors exist (only the formation of non-classical hydrogen bonds is possible).

Taking into account the Pb–O and Pb–N coordination bonds of length in the range of 2.234–2.523 Å, the lead(II) complex has a hemidirected coordination geometry of Pb cation

Table 1. Crystal and refinement data for **1** and **2**.

Empirical formula	$C_{13}H_9N_3O_2Pb$ (**1**)	$C_{13}H_{10}N_6O_{11}Pb$ (**2**)
Formula weight	446.42	633.46
Crystal system	Monoclinic	Monoclinic
Space group	$P2_1/c$	$P2_1/n$
Unit cell dimensions		
a (Å)	11.1911(5)	9.5651(6)
b (Å)	8.5189(3)	7.0159(6)
c (Å)	13.6449(6)	27.861(2)
β (°)	111.538(6)	93.478(7)
Volume (Å^3)	1210.02(9)	1866.2(3)
Z	4	4
Absorption coefficient (mm^{-1})	13.943	9.116
F (0 0 0)	824	1200
Theta range for data collection (°)	1.96–36.36	2.21–25.05
Index ranges	$-14 \le h \le 18$	$-11 \le h \le 8$
	$-12 \le k \le 11$	$-7 \le k \le 8$
	$-22 \le l \le 18$	$-32 \le l \le 32$
Goodness-of-fit on F^2	1.102	1.004
Final R indices [$I > 2\sigma(I)$]	$R_1 = 0.0629$, $wR_2 = 0.0880$	$R_1 = 0.0569$, $wR_2 = 0.1401$
R indices (all data)	$R_1 = 0.1439$, $wR_2 = 0.1154$	$R_1 = 0.0799$, $wR_2 = 0.1472$
Largest diff. peak and hole (e/Å^{-3})	1.705 and −1.876	2.336 and −5.082

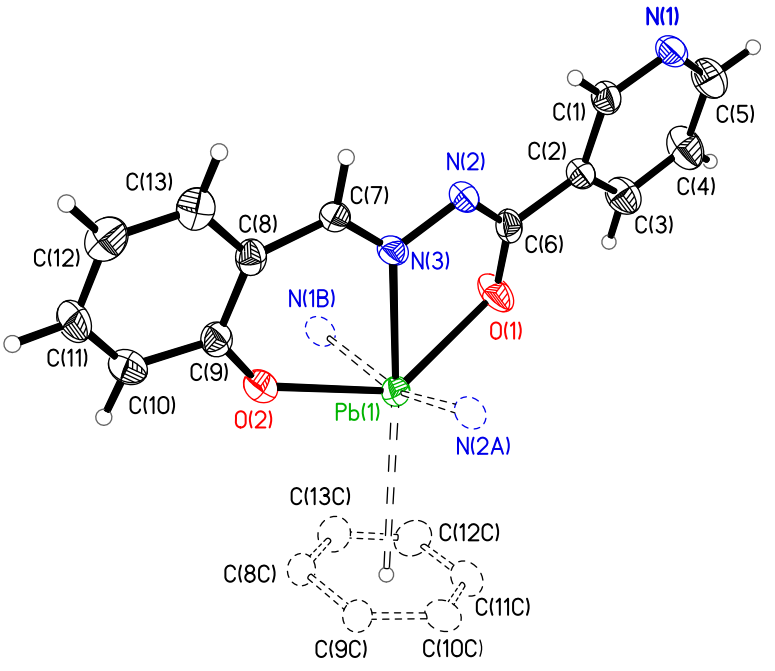

Figure 1. The molecular structure of **1**. Solid lines indicate the content of the asymmetric unit (symmetry codes: N2A: $-x, -y-1, -z+1$; N1B: $x, -y-1/2, z-1/2$; C8C–C13C: $-x, y-1/2, -z+1/2$). The displacement ellipsoids are drawn at 50% probability.

Table 2. Selected geometrical parameters.

Bond length (Å)	**1**	Bond length (Å)	**2**	Free ligand [24]
C6–O1	1.272(9)	C6–O1	1.248(13)	1.222(1)
C9–O2	1.312(10)	C9–O2	1.366(14)	1.354(1)
C6–N2	1.313(10)	C6–N2	1.339(14)	1.354(1)
N2–N3	1.393(9)	N2–N3	1.414(14)	1.375(1)
C7–N3	1.270(10)	C7–N3	1.296(15)	1.276(2)
Pb1–O1	2.428(6)	Pb1–O43	2.460(9)	
Pb1–O2	2.233(6)	Pb1–O41	2.792(11)	
Pb1–N1^{i}	2.523(6)	Pb1–O1	2.477(9)	
Pb1–N3	2.400(6)	Pb1–O22	2.903(9)	
		Pb1–O21	2.977(9)	
		Pb1–O2	2.746(8)	
		Pb1–N3	2.764(10)	
		Pb1–O22^{ii}	2.603(8)	
		Pb1–O23^{ii}	2.938(9)	
		Pb1–O31	3.152(11)	

Note: Symmetry codes: (i) $x, -y-1/2, z-1/2$; (ii) $-x+1/2, y+1/2, -z+1/2$.

[28]. Such arrangement of the N_2O_2 donors can suggest the presence of a gap in the lead (II) coordination sphere; but the phenylene ring centroid is situated at a distance of 3.227 (9) Å from the Pb atom, with an angle of 81.9(6)° between this ring plane and the vector linking the ring centroid – Pb (figure 1). Pb–C distances span a wide range from 3.336 to 3.653 Å and they are shorter than the sum of the Pb and C van der Waals radii (3.72 Å [29]). Similar Pb$\cdots\pi$ interactions have been previously observed in coordination compounds [30–34]. The above-mentioned phenylene ring forms $\pi\cdots\pi$ stacking interactions with pyridine ring of adjacent Pb-salicylaldehyde nicotinoylhydrazone oriented in the opposite direction (figure 2). The distance between ring centroids related by the symmetry operator $(-x, -y-1, -z+1)$ is 3.745(5) Å. Usually, $\pi\cdots\pi$ stacking interactions have a synergistic effect on forming metal ion–π interactions (figure 3), augmenting each other. This cooperative effect of non-covalent interactions has been observed for cation$\cdots\pi$ and halogen$\cdots\pi$ interactions [35–38]. A search of the Cambridge Structural Database (CSD, version 5.33) [1] yielded 57 compounds containing Pb atom in close contact with a six-membered aromatic ring (with the Pb within 4 Å from the centroid of the π ring and the angle between the vector linking the ring centroid – Pb and ring plane ranging from 70° to 90°), with the mean Pb$\cdots\pi$ (centroid) distance of 3.488(28) Å. Metal$\cdots\pi$ interactions have been attracting

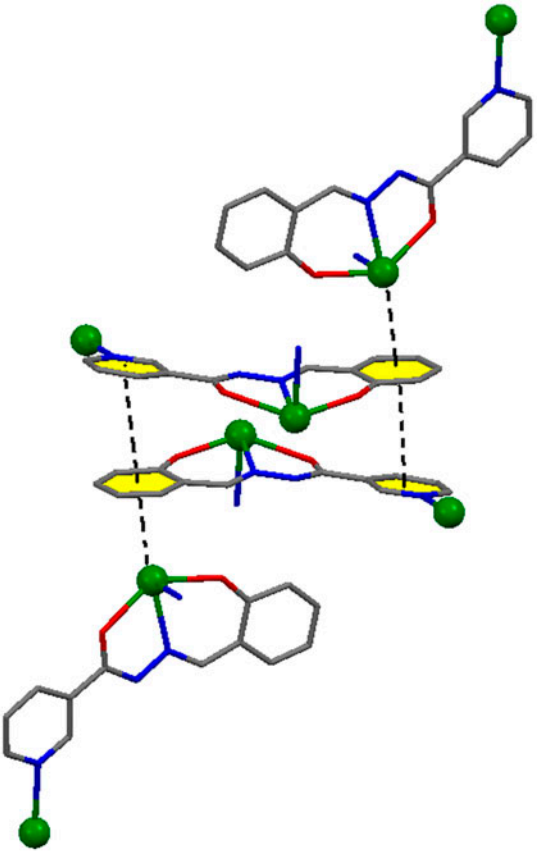

Figure 2. The interplay between the Pb$\cdots\pi$ interactions and the $\pi\cdots\pi$ stacking interactions.

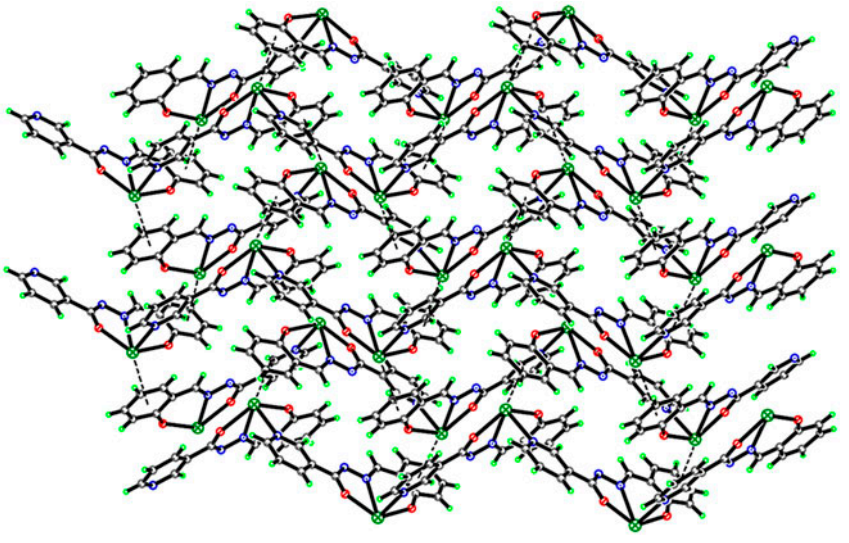

Figure 3. Part of molecular packing of **1** showing Pb$\cdots\pi$ interactions viewed along the *bc* plane.

increasing attention in supramolecular chemistry, crystal engineering, and organometallic chemistry [30, 39–42]. The DFT/MP2 calculated energy of $Pb^{2+}\cdots\pi$ interaction [for the isolated model of Pb$\cdots$benzene moiety possessing geometrical parameters taken from the structure of **1** (figure S7, table S1)] is 60 kcal/mol and this interaction has a bonding character. The literature has reported gas-phase binding energies of metal cation–arene complexes varying from 20 kcal/mol (for s-block element ions [37, 43]) to about 200 kcal/mol (for transition metal ions) [44, 45]. These gas-phase binding energy values calculated for model metal ion$\cdots$benzene moieties are similar to the experimentally determined values of bond dissociation energies [46, 47]. In general, metal ion$\cdots\pi$ interactions are one of the strongest non-covalent interactions [37, 40] and the electrostatic contribution plays an important role in binding energies.

There is one more possible interaction between the lead(II) ion and the organic ligand that can be considered. In the structure there was observed a short contact (2.976 Å) between Pb(II) ion and the hydrazone nitrogen atom (N2) of the neighboring molecule related by the symmetry operator ($-x$, $-y-1$, $-z+1$) (figure 1). Such coordination sphere bond distance is typical for coordination compounds of lead; however, in such cases the lone pair of electrons on sp^2-hybridized nitrogen and the Pb–N bond are co-planar. Since in **1** the electron density is delocalized within the N2–C6–O1 moiety, there is a possibility that N2 atom forms secondary interaction with Pb atom. The two neighboring molecules are connected by $\pi\cdots\pi$ stacking interactions between phenylene rings and pyridine rings. The $\pi\cdots\pi$ stacking interactions, in this case, induce a short contact between the Pb(II) ion and the hydrazone nitrogen atom (N2), and in consequence force the Pb–N interaction. The existence of secondary Pb–N/O interactions was observed in several lead(II) compounds [3, 48–52]. The coordination of lead(II) in **1** can be classified as holodirected and the dimensionality of **1** changes from 1-D to 2-D.

To gain insight into the lead(II) ion interaction properties (figure S8), the topological analysis of the electron density distributions was performed using Bader's theory of atoms in molecules [53]. The values of electron density (ρ_C) (table 3) for bond and cage critical

points indicate that Pb–C and Pb–N2 interactions exist and they are weaker than the Pb–N/O coordination bonds involved in the lead(II) coordination sphere. The positive value of total electron energy density at bond critical point (H_C) indicates that the Pb–C interaction has non-covalent character. For Pb–N/O bonds, the values of Laplacian electron densities at bond critical points ($\nabla^2\rho_C$) are also positive but values of total electron energy densities at these bond critical points are negative, suggesting partially covalent character of these interactions.

The similar reaction between lead(II) acetate and *para*-isomer of nicotinic acid hydrazone gave the *catena*-[(μ_2-*N*-((2-oxidophenyl)methylidene)pyridine-4-carbohydrazonoato-*N*:*N*′,*O*,*O*′)-lead(II) methanol solvate] [54]. This compound creates, analogous to **1**, linkage via primary interactions but the molecules are differently arranged in the crystal net. In **1** the molecules propagate creating zigzag chains, while in the *catena*-[(μ_2-*N*-((2-oxidophenyl)methylidene)pyridine-4-carbohydrazonoato-*N*:*N*′,*O*,*O*′)-lead(II) methanol solvate] molecules create trigonal tube structure and are related by 3_1 axis (figure 4).

Direct reaction of lead(II) nitrate with *N*′-salicylidene-3-pyridinecarbohydrazide monohydrate yielded the coordination polymer $[Pb(C_{13}H_{10}N_6O_{11})]_n$ **2** (figure 5), wherein one tetradentate nitrate ion (bidentate chelating toward each metal ion) acts as a linker between lead(IV) ions forming 1-D zigzag chains along the crystallographic [0 1 0] axis (the same structural motif as in **1**) (figure 6). The chains are interlinked by weak $\pi\cdots\pi$ stacking interactions between phenylene and pyridine rings of organic ligands, and N–H···O hydrogen bonds between amide groups and coordinated nitrates functioning as linkers. The presence of oxidizing agents in the reaction environment caused the change in lead oxidation state from +2 to +4.

The coordination sphere of lead(IV) contains the monoanionic ligand (that binds mode), one nitrate ion as a bidentate chelating ligand, and two bridging nitrate ligands (one from neighboring asymmetric unit) with both acting as bidentate chelating toward this one lead ion (figure 5). The three coordination bonds of the bridging–chelating system are distinctly weaker than the remaining ones (table 2), but considering the nitrate ion as bonded jointly via two Pb–O bonds this ligand can be considered as bonded stronger than the typical monodentate O-donor ligand. The charge of complex cation is balanced by the presence of third nitrate ion completing the coordination sphere of lead(IV) via weak Pb–O interaction (3.152(11) Å, table 2). Although the longest Pb(IV)–O(nitrate) distances of **2** exceed the Pb(IV)–O bond length range of 2.1–2.9 Å recorded on the CSD [1], they are smaller than the sum of the van der Waals radii (3.52 Å [29]). Thus, lead(IV) ion is ten-coordinate and exhibits a holodirected coordination geometry. The lead atom of **2** adopts bicapped tetragonal prismatic distorted toward bicapped tetragonal antiprismatic coordination geometry, with

Table 3. Topological parameters of the lead(II) coordination sphere [the electron density at bond critical point BCP (ρ_C), its Laplacian ($\nabla^2\rho_C$), the kinetic electron energy density (G_C), the potential electron energy density (V_C), and the total electron energy density at BCP (H_C)]; all values are given in a.u.

	$\nabla^2\rho_C$	ρ_C	G_C	V_C	H_C
Pb1–O1	0.0436	0.0458	0.0448	−0.0461	−0.0013
Pb1–N3	0.0503	0.0541	0.0531	−0.0559	−0.0028
Pb1–O2	0.0830	0.0647	0.0838	−0.0846	−0.0008
Pb1–N1^{i}	0.0344	0.0427	0.0358	−0.0373	−0.0015
Pb1–C8^{ii}	0.0069	0.0129	0.0065	−0.0061	0.0004
Pb1–N2^{iii}	0.0105	0.0201	0.0110	−0.0116	−0.0006

Note: Symmetry codes: (i) x, $-y-1/2$, $z-1/2$; (ii) $-x$, $y-1/2$, $-z+1/2$; (iii) $-x$, $-y-1$, $-z+1$.

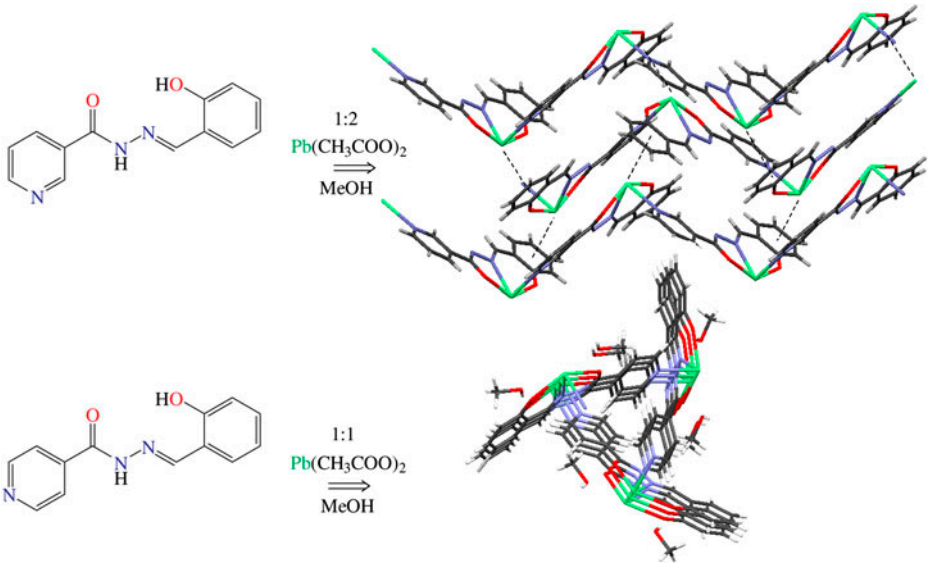

Figure 4. The crystal packing of lead(II) coordination compounds, **1** and *catena*-[(μ_2-*N*-((2-oxidophenyl) methylidene)pyridine-4-carbohydrazonoato-*N*:*N*′,*O*,*O*′)-lead(II) methanol solvate] [48].

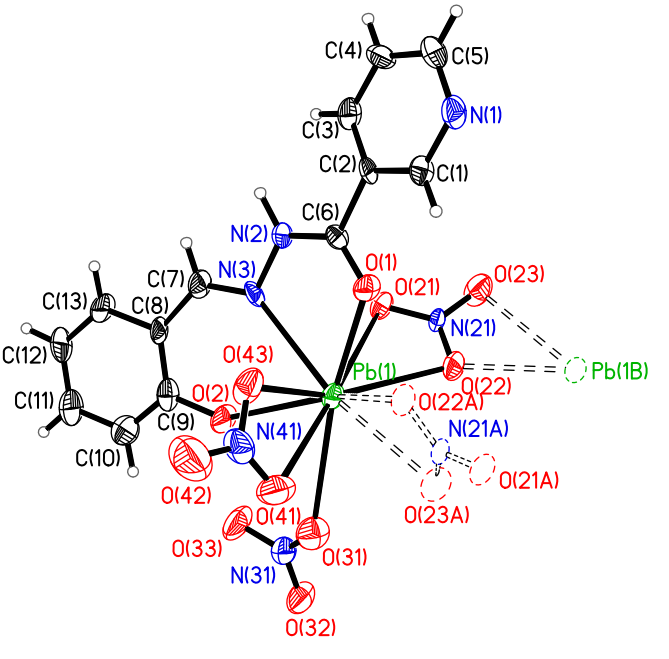

Figure 5. The molecular structure of **2**. Solid lines indicate the content of the asymmetric unit (symmetry codes: N21A, O21A, O22A, O23A: $-x+1/2$, $y+1/2$, $-z+1/2$; Pb1B: $-x+1/2$, $y-1/2$, $-z+1/2$). The displacement ellipsoids are drawn at 50% probability.

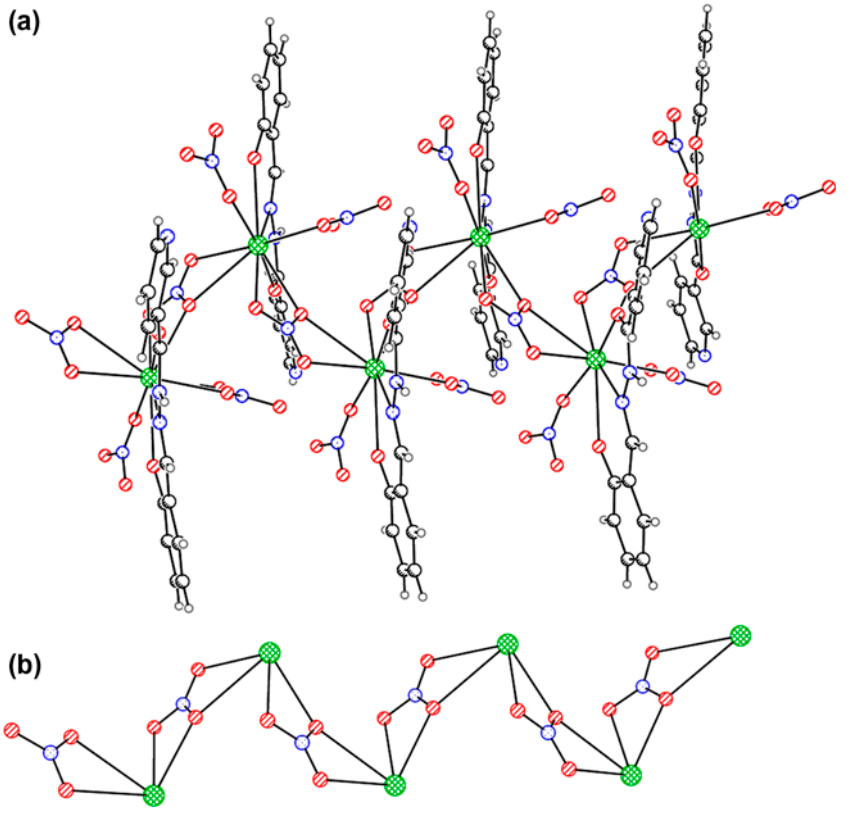

Figure 6. The 1-D zigzag chain (a) formed by the bidentate chelating nitrates (b).

N3 and O23 atoms (generated by symmetry operator: $-x+1/2$, $y+1/2$, $-z+1/2$) occupying apical positions. Two nitrate ions coordinate asymmetrically, with the difference of distances between Pb atom and the two O atoms of the same nitrate group of ca. 0.33 Å. The third chelating nitrate ion is bounded symmetrically. The weakly bonded monodentate nitrate ion is separated from another, symmetry generated, monodentate nitrate ion by a distance of 2.843(19) Å existing between O32···O32^{i} (symmetry code: (i) $-x$, $-y$, $-z$) and from the phenolate O atom by a distance of 2.569(14) Å between O33···O2 atoms. The O···O distance fulfills the criterion of being shorter than the sum of the O van der Waals radii (3.04 Å [29]). Although in some systems the O···O interactions have repulsive character [55], the importance of non-covalent O···O interaction in supramolecular architectures is well established.

Complexation does not induce conformational changes of the ligand, in contrast to **1**. The ligand bond lengths in **2** are consistent with those in the uncoordinated hydrazone [24], except for the C(O)N (table 2). The C–N bond is shortened and the C–O bond is elongated in **2**, in comparison to free hydrazone, but the differences between bond lengths are smaller than for **1**. A search of the CSD [1] yielded 141 coordination compounds containing the acyl hydrazone of salicylaldehyde (keto form). The average C=O and C–N distances from 228 hits is 1.250(1) and 1.332(1) Å, respectively, and these distances are slightly shorter than those observed in **2**. An analogous search carried out for an enol

form gives 589 compounds, with 959 different bonds with a mean distance of 1.299(1) Å for C–O and 1.272(1) Å for C=N bonds. Thus, the hydrazone in **2** exists in the rarely adopted keto form. The ligand is distorted from planarity. The dihedral angle formed by the weighted least-squares planes defined by the atoms of pyridine and phenylene is 24.48 (26)°. There are no Pb$\cdots\pi$ interactions because of the presence of coordinated nitrates in the lead(IV) coordination sphere.

3.2. *Spectroscopic studies*

IR spectra (figure S3) of both compounds contain characteristic bands of the stretching and bending vibrations of the C=C, C=N, and CH groups. The C–H stretching vibrations are assigned to the bands at 3040–3250 cm^{-1}. The differences in the ligand coordination mode influence the position of some bands in the IR spectra. The absence of the band corresponding to C=O stretching vibrations of C(O)NH group and the small hypsochromic shift (in comparison to free ligand) of the band attributed to $C=N_{imine}$ stretching vibrations (1605 cm^{-1}) is consistent with the coordination of nicotinoylhydrazone for **1**. For free ligand [24], C=N stretching mode is observed at 1600 cm^{-1} (figure S4). The ligand exists in the enolate form in the complex, confirmed by the presence of an additional band in the spectrum of **1** at 1355 cm^{-1} assigned to the $C–O_{enolate}$ stretching vibrations. An additional band at 1465 cm^{-1} in the spectrum of **1** corresponds to the stretching vibration of C=N of the N=C–O moiety and $C–O_{phenolate}$ bond. The IR spectrum of **2** contains a strong band at 1650 cm^{-1} originating from the bending vibrations of N–H and stretching vibrations of C=O, corresponding to bonding of the ligand to the metal in the keto form. There are no bands corresponding to the stretch of the hydrazinic N–H bond for **1**, whereas N–H stretching vibrations are assigned to the band at 3450 cm^{-1} for **2**. The N–N stretching vibrations appear as a weak band. The appearance of bands corresponding to Pb–N and Pb–O bonds confirms the presence of coordination bonds. The spectrum of **2** exhibits additional bands corresponding to vibrations of chelating bidentate nitrate bonds (1480 cm^{-1} and 1290 cm^{-1}). Most of the vibrational modes are strongly overlapped and only the predominant contributions are indicated in table 4.

UV–Vis spectra (figure 7), recorded for the solid-state samples, exhibit four principal absorption bands for **1** and three absorption bands for **2**. For **1**, the strong band located at 370 nm with shoulders at 210 and 290 nm can be attributed to $\pi \rightarrow \pi^*$ transitions. The band centered at 440 nm can be considered as a charge transfer transition involving ligand-to-metal π electron donation [56]. In the UV–Vis spectrum of **2** there is an intense absorption at 355 nm with shoulders at 220 and 290 nm, which can be assigned to $\pi \rightarrow \pi^*$ transitions. *N*-salicylidene-3-pyridinecarbohydrazide in the solid state exhibits two absorptions at 270 and 325 nm, attributed to $\pi \rightarrow \pi^*$ transitions within azomethine C=N bond and aromatic rings.

3.3. *Thermal stability*

The thermal decomposition of *N*-salicylidene-3-pyridinecarbohydrazide is a multi-stage process (figure S5). The ligand is stable up to 55 °C in air. This first endothermic step is attributed to removal of water molecule (mass loss of 7.0%) at 55–160 °C. The DTA (75–130 °C) and DTG (minima at 106 °C, 120 °C) curves indicate that there are two sub-processes in this step. The second endothermic step occurs without mass loss and it

Table 4. The principal vibrational frequencies (cm^{-1}) with the assignment.

$\nu_{exp.}$ 1	Assignment	$\nu_{exp.}$ 2	Assignment	$\nu_{exp.}$ ligand	Assignment
3070, 3040	ν(CH)	3450	ν(NH)	3480	ν_{as}(OH), ν_{s}(OH)
1605	ν(CN)	3250, 3070	ν(CH)	3250–3100	ν(NH), ν(CH)
1600	ν(CC)	1650	ν(CO), δ(NH)	3050	ν(CH)
1520	ν(CC)	1610	ν(CN)	1670, 1655, 1650	ν(CO), δ(NH)
1465	ν(CN), ν(CO)	1595, 1550	ν(CC)	1620, 1610	δ(NH), δ(OH)
1440	δ(CH), ν(CC)	1480	$\nu(NO_3)$, δ(NH), ν(CO), ν(CC)	1600	ν(CC), ν(CN)
1365, 1355, 1350	ν(CO), δ(CH), δ(CC)	1440	δ(CH), ν(CC)	1575	δ(CH)
1245	δ(CH)	1420	δ(CH)	1555	δ(NH), δ(OH), δ(CH), ν(CC)
1190	δ(CH), δ(CC)	1385	δ(NH), δ(CH), δ(CC)	1490	δ(OH), δ(CH)
1150	δ(CH)	1290	$\nu(NO_3)$, ν(CO), δ(CH)	1480	ν(CO), ν(CC), ν(CN)
1007	δ(CC), δ(CN), ν(NN)	1210, 1200	δ(CH), δ(CC)	1425	δ(CH)
960	δ(CH)	1160	δ(CC), δ(CH)	1380	δ(OH)
930	δ(CC), δ(CN), δ(CONN)	1130	δ(CH)	1355	δ(CH)
885	δ(CC), δ(CN)	1045	$\nu(NO_3)$	1335	ν(CO), δ(CH)
760	δ(CH)	1030, 1020	δ(CC), δ(CN), ν(NN)	1290	δ(CC)
730	δ(CH)	930	δ(CC), δ(CN)	1240	δ(CH), δ(NH), δ(NCO)
640	δ(CH)	880	δ(CC), δ(CN)	1205	δ(CC), δ(CH)
620	δ(CC)	820	$\nu(NO_3)$	1155	δ(CH)
580	δ(CC), ν(PbO)	750	δ(CH)	1135	δ(CH), ν(NN)
510	δ(CC), δ(CO), ν(PbO)	720	$\delta(NO_3)$	1120	δ(CH)
475	δ(CC)	690	δ(CH)	1030	δ(CC)
450	δ(CH)	635	δ(CH), δ(CC)	960	δ(NH), δ(OH), δ(CH)
420	ν(PbN), δ(CH)	590	ν(PbO)	920	δ(NH), δ(OH), δ(CH)
380	δ(CH)	500	ν(PbO)	875	δ(CC), δ(NCO)
		440	ν(PbN)	760	δ(CH)
				700	δ(CC), δ(CN)
				670	δ(CC)

corresponds to the melting of anhydrous ligand (minimum at 188 °C on the DTA curve). The succeeding stage (161–390 °C) is characterized by strong, narrow peaks on the DTG curve (325 °C) and the biggest mass loss (57.3%). The last stage of decomposition is exothermic and it occurs from 391 °C (minimum at 490 °C on the DTG curve) to 550 °C (maximum at 500 °C on the DTA curve). The total mass loss of 100% corresponds to the total decomposition of ligand above 550 °C.

Compound **1** is thermally more stable than pure ligand (figure S6) in air and its decomposition occurs in two exothermic stages. The first step of the thermal decomposition takes place within the temperature range of 45–390 °C. This step is characterized by strong, narrow peaks on the DTA curve (355 °C) and the DTG curve (350 °C). The second step of thermal decomposition occurs from 391 to 480 °C. The DTA (443 °C) and DTG (minimum at 440 °C) curves indicate that this is a one-stage process. Over 480 °C, **1** decomposes to PbO, which was determined on the basis of mass loss (calculated 49.5%, theoretical 50%).

The lead(IV) compound **2** is thermally less stable than **1** (figure S6). All decomposition stages are exothermic. The TGA curve exhibits three distinct weight loss steps. The decom-

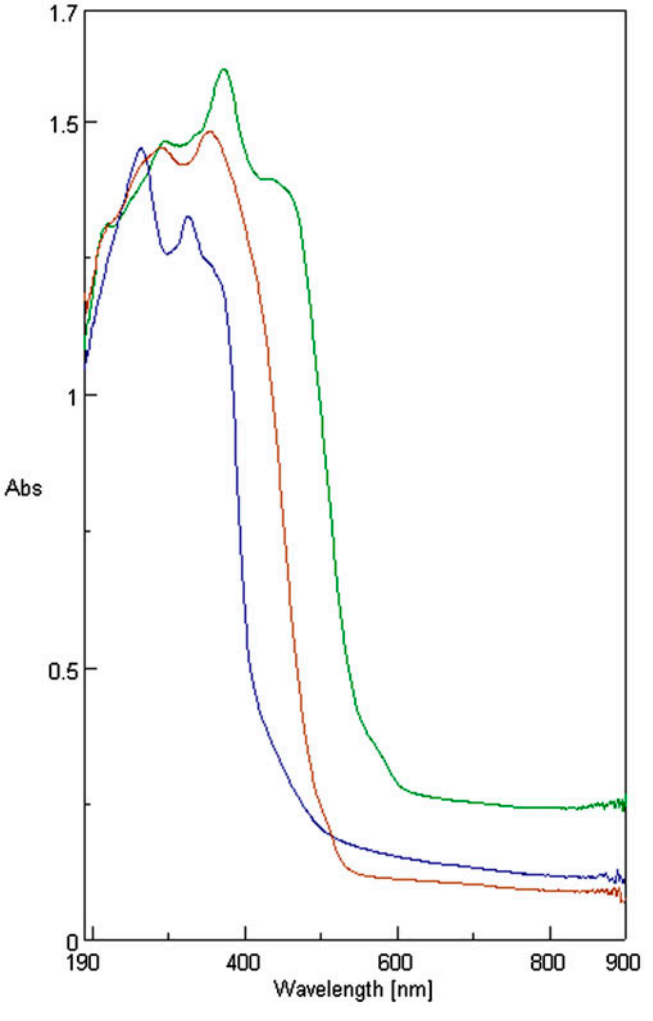

Figure 7. The solid-state UV–Vis spectra of **1** (green line), **2** (red line) and ligand (blue line) (see http://dx.doi.org/10.1080/01694243.2012.735194 for color version).

position starts at 260 °C and ends at 510 °C with weight loss of 60.8%. The first step of the decomposition is characterized by strong, narrow peaks on the DTA curve (300 °C) and the DTG curve (300 °C), and originates from decomposition of ligand. The second step is combined with the third one and corresponds to the simultaneous decomposition of nitrate and organic ligand. The last stage of decomposition occurs from 390 °C (minimum at 480 °C on the DTG curve) to 510 °C (maximum at 480 °C on the DTA curve).

4. Conclusion

The syntheses of lead coordination compounds with *N*′-(2-hydroxybenzylidene)nicotinohydrazide were performed in the same experimental conditions. Lead(II) acetate yielded a 2-D lead(II) coordination polymer (**1**), in which the hydrazone is a linker. The formation of

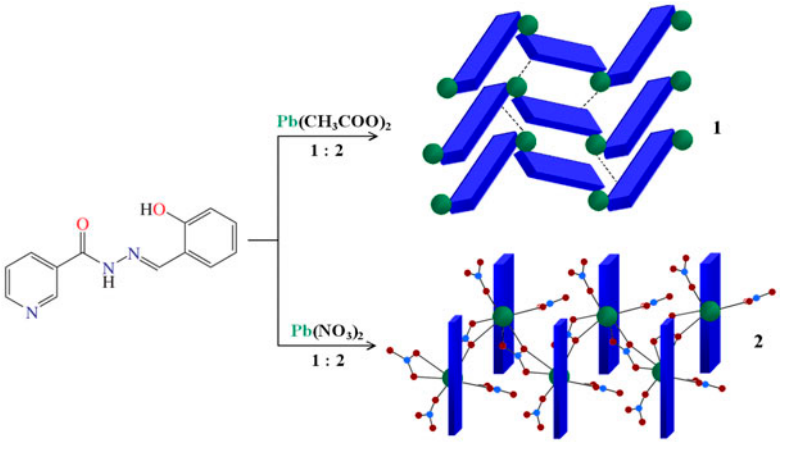

Scheme 1. Comparison of syntheses of lead coordination compound with nicotinoylhydrazone (blue rectangular prism: organic ligand, green sphere: lead ion). The Pb···π interactions are indicated by dashed lines (see http://dx.doi.org/10.1080/00958972.2013.876494 for color version).

metal-organic framework of **1** is affected by Pb···π interactions. Using lead(II) nitrate during synthesis led to the formation of a 1-D lead(IV) coordination polymer (**2**), in which nitrates bridge between lead(IV) centers (scheme 1).

Although the coordination bonds are the primary interactions in coordination polymers, the non-covalent interactions often play important roles in the extension of a coordination network into larger architecture. The 2-D coordination polymer of lead(II) (**1**) exhibits, in addition to coordination bonds, two types of non-covalent interactions, π···π stacking and Pb···π interactions. The Pb···π interactions, although rarely observed and recognized in solid-state structures of lead(II) compounds [29], should be considered as supramolecular bonding interactions in studies of interaction mechanisms of lead and in designing new lead compounds. The synergic effect of π···π interactions on the Pb···π bonds cannot be neglected. Metal···π interactions should be taken into account in the structural chemistry of nicotinoylhydrazones and more complex compounds containing nicotinoylhydrazone, as well as in any complete analysis of their coordination properties [57–59].

Supplementary material

CCDC-926481 (**1**) and CCDC-967624 (**2**) contain the supplementary crystallographic data for this article. These data can be obtained free of charge via http://www.ccdc.cam.ac.uk/conts/retrieving.html [or from the Cambridge Crystallographic Data Center (CCDC), 12 Union Road, Cambridge CB2 1EZ, UK; Fax: +44(0)1223–336033; E-mail: deposit@ccdc.cam.ac.uk].

Acknowledgments

This research was supported by the Institute of General and Ecological Chemistry, TUL (statutory sources), and the Faculty of Chemistry, Lodz University of Technology (Young Scientists' Fund). The GAUSSIAN03 calculations were carried out in the Academic Computer Centre CYFRONET of the AGH University of Science and Technology in Cracow, Poland (grant number: MNiSW/SGI3700/PŁódzka/040/2008).

References

[1] F.H. Allen. *Acta Crystallogr., Sect. B: Struct. Sci.*, **58**, 380 (2002).
[2] G. Zampella, K.P. Neupane, L. De Gioia, V.L. Pecoraro. *Chem. Eur. J.*, **18**, 2040 (2012).
[3] D.-Q. Li, X. Liu, J. Zhou. *Inorg. Chem. Commun.*, **11**, 367 (2008).
[4] F. Marandi, J. Sartaji, G. Bruno, H.A. Rudbari. *J. Coord. Chem.*, **65**, 1872 (2012).
[5] R.L. Davidovich, V. Stavila, D.V. Marinin, E.I. Voit, K.H. Whitmire. *Coord. Chem. Rev.*, **253**, 1316 (2009).
[6] R.L. Davidovich, V. Stavila, K.H. Whitmire. *Coord. Chem. Rev.*, **254**, 2193 (2010).
[7] M.-L. Hu, A. Morsali, L. Aboutorabi. *Coord. Chem. Rev.*, **255**, 2821 (2011).
[8] S.-H. Li, S.-K. Gao, S.-X. Liu, Y.-N. Guo. *Cryst. Growth Des.*, **10**, 495 (2010).
[9] W. Liang, Z. Zhong, Z.-C. Pan, Q.-H. Meng, Y. Deng, K.-L. Zhang. *J. Coord. Chem.*, **66**, 2802 (2013).
[10] Z. Wang, Q. Wei, G. Xie, Q. Yang, S. Chen, S. Gao. *J. Coord. Chem.*, **65**, 286 (2012).
[11] J.S. Magyar, T.-C. Weng, C.M. Stern, D.F. Dye, B.W. Rous, J.C. Payne, B.M. Bridgewater, A. Mijovilovich, G. Parkin, J.M. Zaleski, J.E. Penner-Hahn, H.A. Godwin. *J. Am. Chem. Soc.*, **127**, 9495 (2005).
[12] C. Gourlaouen, O. Parisel. *Angew. Chem. Int. Ed.*, **46**, 553 (2007).
[13] G.M. Sheldrick. *Acta Crystallogr., Sect. A*, **64**, 112 (2008).
[14] SETSOFT. *Software (Version 3.0, Revision 2)*, SETARAM Instrumentation, Caluire, France (2000).
[15] Y. Zhao, D.G. Truhlar. *Theor. Chem. Acc.*, **120**, 215 (2008).
[16] M. Head-Gordon, T. Head-Gordon. *Chem. Phys. Lett.*, **220**, 122 (1994).
[17] M.J. Frisch, G.W. Trucks, H.B. Schlegel, G.E. Scuseria, M.A. Robb, J.R. Cheeseman, G. Scalmani, V. Barone, B. Mennucci, G.A. Petersson, H. Nakatsuji, M. Caricato, X. Li, H.P. Hratchian, A.F. Izmaylov, J. Bloino, G. Zheng, J.L. Sonnenberg, M. Hada, M. Ehara, K. Toyota, R. Fukuda, J. Hasegawa, M. Ishida, T. Nakajima, Y. Honda, O. Kitao, H. Nakai, T. Vreven, J.A. Montgomery, Jr., J.E. Peralta, F. Ogliaro, M. Bearpark, J.J. Heyd, E. Brothers, K.N. Kudin, V.N. Staroverov, R. Kobayashi, J. Normand, K. Raghavachari, A. Rendell, J.C. Burant, S.S. Iyengar, J. Tomasi, M. Cossi, N. Rega, J.M. Millam, M. Klene, J.E. Knox, J.B. Cross, V. Bakken, C. Adamo, J. Jaramillo, R. Gomperts, R.E. Stratmann, O. Yazyev, A.J. Austin, R. Cammi, C. Pomelli, J.W. Ochterski, R.L. Martin, K. Morokuma, V.G. Zakrzewski, G.A. Voth, P. Salvador, J.J. Dannenberg, S. Dapprich, A.D. Daniels, O. Farkas, J.B. Foresman, J.V. Ortiz, J. Cioslowski, D.J. Fox, *Gaussian 09, Revision A.02*, Gaussian, Inc., Wallingford, CT (2009).
[18] S.F. Boys, F. Bernardi. *Mol. Phys.*, **19**, 553 (1970).
[19] F. Biegler-König, J. Schönbohm. *AIM2000 – A Program to Analyze and Visualize Atoms in Molecules*, Büro Streibel Biegler-König, Innovative Software, Bielefeld, Germany.
[20] S. Huzinaga, B. Miguel. *Chem. Phys. Lett.*, **175**, 289 (1990).
[21] S. Huzinaga, M. Klobukowski. *Chem. Phys. Lett.*, **212**, 260 (1993).
[22] D. Feller. *J. Comp. Chem.*, **17**, 1571 (1996).
[23] K.L. Schuchardt, B.T. Didier, T. Elsethagen, L. Sun, V. Gurumoorthi, J. Chase, J. Li, T.L. Windus. *J. Chem. Inf. Model.*, **47**, 1045 (2007).
[24] N. Galić, B. Perić, B. Kojić-Prodić, Z. Cimerman. *J. Mol. Struct.*, **559**, 187 (2001).
[25] M.R. Maurya, S. Agarwal, C. Bader, M. Ebel, D. Rehder. *Dalton Trans.*, 537 (2005).
[26] E.B. Seena, N. Mathew, M. Kuriakose, M.R.P. Kurup. *Polyhedron*, **27**, 1455 (2008).
[27] Q.-F. Zhang, F.-L. Jiang, Y.-G. Huang, W. Wei, Q. Gao, M. Yang, K.-C. Xiong, M.-C. Hong. *Dalton Trans.*, 2673 (2009).
[28] L. Shimoni-Livny, J.P. Glusker, C.W. Bock. *Inorg. Chem.*, **37**, 1853 (1998).
[29] A. Bondi. *J. Phys. Chem.*, **68**, 441 (1964).
[30] E.R.T. Tiekink, J. Zukerman-Schpector. *Aust. J. Chem.*, **63**, 535 (2010).
[31] H. Schmidbaur, A. Schier. *Organometallics*, **27**, 2361 (2008).
[32] J.-K. Cheng, X. Zhang, M.-J. Zhang, Y.-G. Yao. *Inorg. Chem. Commun.*, **17**, 88 (2012).
[33] A.G. Gash, P.F. Rodesiler, E.L. Amma. *Inorg. Chem.*, **13**, 2429 (1974).
[34] J.M. Harrowfield, S. Maghaminia, A.A. Soudi. *Inorg. Chem.*, **43**, 1810 (2004).
[35] D. Escudero, A. Frontera, D. Quiñonero, P.M. Deyà. *J. Comput. Chem.*, **30**, 75 (2009).
[36] Y.N. Imai, Y. Inoue, I. Nakanishi, K. Kitaura. *Protein Sci.*, **17**, 1129 (2008).
[37] S. Reddy, D. Vijay, G. Sastry, G. Sastry. *J. Phys. Chem. B*, **110**, 2479 (2006).
[38] R. Kruszynski, A. Trzesowska-Kruszynska. *Acta Crystallogr., Sect. C: Cryst. Struct. Commun.*, **66**, o449 (2010).
[39] E.R.T. Tiekink, J. Zukerman-Schpector. *The Importance of Pi-Interactions in Crystal Engineering*, Wiley, Chichester (2012).
[40] A.Yu. Rogachev, M.A. Petrukhina. *J. Phys. Chem. A*, **113**, 5743 (2009).
[41] I. Caracelli, J. Zukerman-Schpector, E.R.T. Tiekink. *Coord. Chem. Rev.*, **256**, 412 (2012).
[42] E.R.T. Tiekink, J. Zukerman-Schpector. *CrystEngComm*, **11**, 1176 (2009).
[43] P. Kadlubanski, K. Calderón-Mojica, W.A. Rodriguez, D. Majumdar, S. Roszak, J. Leszczynski. *J. Phys. Chem. A*, **117**, 7989 (2013).
[44] H.-B. Yi, H.M. Lee, K.S. Kim. *J. Chem. Theory Comput.*, **5**, 1709 (2009).

[45] H.-B. Yi, M. Diefenbach, Y.C. Choi, E.C. Lee, H.M. Lee, B.H. Hong, K.S. Kim. *Chem. Eur. J.*, **12**, 4885 (2006).
[46] J.C. Amicangelo, P.B. Armentrout. *J. Phys. Chem. A*, **104**, 11420 (2000).
[47] P.B. Armentrout, M.T. Rodgers. *J. Phys. Chem. A*, **104**, 2238 (2000).
[48] J. Shi, J.-W. Ye, T.-Y. Song, D.-J. Zhang, K.-R. Ma, J. Ha, J.-N. Xu, P. Zhang. *Inorg. Chem. Commun.*, **10**, 1534 (2007).
[49] A.A. Soudi, F. Marandi, A. Morsali, L.-G. Zhu. *Inorg. Chem. Commun.*, **8**, 773 (2005).
[50] E. López-Torres, M.A. Mendiola. *Dalton Trans.*, 7639 (2009).
[51] Y.-Z. Yuan, J. Zhou, X. Liu, L.-H. Liu, K.-B. Yu. *Inorg. Chem. Commun.*, **10**, 47 (2007).
[52] Y.-Y. Zhang, S.-X. Liu, K.-K. Du, M.-X. Xue. *Inorg. Chem. Commun.*, **13**, 641 (2010).
[53] R.W.F. Bader. *Atoms in Molecules: A Quantum Theory*, Clarendon, Oxford (1990).
[54] G.H. Shahverdizadeh, S.W. Ng, E.R.T. Tiekink, B. Mirtamizdoust. *Acta Crystallogr., Sect. E: Struct. Rep. Online*, **67**, m1583 (2011).
[55] A. Das, S.R. Choudhury, B. Dey, S. Yalamanchili, M. Helliwell, P. Gamez, S. Mukhopadhyay, C. Estarellas, A. Frontera. *J. Phys. Chem. B*, **114**, 4998 (2010).
[56] H.L. Singh, J.B. Singh. *Int. J. Inorg. Chem.*, Article ID 568797, **2012**, 7 (2012).
[57] S.-Z. Bai, X.-H. Lou, H.-M. Li, H. Shi. *Acta Crystallogr., Sect. E: Struct. Rep. Online*, **65**, m842 (2009).
[58] S. Ghammamy, H. Sahebalzamani, N. Khaligh, R. Rahimi. *Acta Crystallogr., Sect. E: Struct. Rep. Online*, **66**, m294 (2010).
[59] H. Grove, T.L. Kelly, L.K. Thompson, L. Zhao, Z. Xu, T.S.M. Abedin, D.O. Miller, A.E. Goeta, C. Wilson, J.A.K. Howard. *Inorg. Chem.*, **43**, 4278 (2004).